LES study on turbulent particle deposition and its dependence on atmospheric boundary-layer stability

Xin Yin[1], Cong Jiang[1], Yaping Shao[1], Ning Huang[2], Jie Zhang[2]

[1] Institute for Geophysics and Meteorology, University of Cologne, Cologne, Germany
[2] Key Laboratory of Mechanics on Disaster and Environment in Western China, Lanzhou University, Lanzhou, China

Correspondence to: Jie Zhang (zhang-j@lzu.edu.cn)

Abstract. It is increasingly recognized that atmospheric boundary-layer stability (ABLS) plays an important role in aeolian processes. While the effects of ABLS on particle emission have attracted much attention and been investigated in several studies, those on particle deposition are so far less-well studied. By means of large-eddy simulation, we investigate how ABLS influences the probability distribution of surface shear stress and hence particle deposition. Statistical analysis of the model results reveals that the shear stress can be well approximated by using a Weibull distribution and the ABLS influences on particle deposition can be estimated by considering the shear stress fluctuations. The model-simulated particle depositions are compared with the predictions of a particle-deposition scheme and measurements, and the findings are then used to improve the particle-deposition scheme. This research represents a further step towards developing deposition schemes that account for the stochastic nature of particle processes.

Keywords: Particle deposition, Atmospheric boundary-layer stability, Surface shear stress, Weibull distribution, Stochastic particle process

1 Introduction

Dry deposition is the removal of particulates and gases at the air-surface interface by turbulent transfer and gravitational settling (Sehmel, 1980; Droppo, 2006; Hicks et al., 2016). Because it is the only process for the removal of particles from the atmosphere in the absence of precipitation, developing reliable methods for estimating dry deposition of particles has attracted much interest since the early 1940s (Gregory, 1945; Chamberlain, 1953; Slinn and Slinn, 1980; Slinn, 1982; Walcek et al., 1986; Zhang et al., 2001; Petroff and Zhang, 2010; Zhang and Shao, 2014; Seinfeld et al., 2016). Several particle-deposition schemes have been proposed (Slinn, 1982; Walcek et al., 1986; Zhang and Shao, 2014; Zhang et al., 2001) for regional/global models, which are driven by using several environmental parameters, including the Reynolds surface shear stress (typically averaged over 15-30 min). However, field observations indicate that the use of Reynolds stress as the only wind-related parameter in such schemes may not be sufficient to achieve accurate estimates of particle deposition, because of the nonlinear relationship between deposition velocity and wind shear. The observations using the eddy correlation method show that particle-deposition velocity has strong spatiotemporal variations associated with the fluctuations of wind speed (Connan et al., 2018; Damay et al.,

2009; Lamaud et al., 1994; Wesely et al., 1983, 1985). It is also observed that when the background wind speeds are similar, dry deposition velocities under convective conditions are larger than under neutral and stable conditions (Fowler et al., 2009). Pellerin et al. (2017) suggested that cospectral similarities exist between heat and particle-deposition fluxes and that atmospheric turbulence plays a role in particle deposition. It is therefore necessary to find a link between instantaneous wind and particle deposition and to correctly represent this link in particle-deposition schemes, i.e., to introduce and account for the effect of turbulence on particle deposition.

Some aeolian processes, e.g., turbulent particle emission (Klose and Shao, 2012, 2013) and intermittent saltation (Li et al., 2020; Liu et al., 2018; Rana et al., 2020), have been under development. To the best of our knowledge, although turbulent particle deposition is now perceived to be important, a scheme is yet to be constructed for its quantitative estimate.

The turbulent wind flow in a particle-deposition scheme is reflected in the turbulent shear stress (or vertical momentum flux) (Fowler et al., 2009; Zhang and Shao, 2014). It is well-known that apart from gravitational settling, particle deposition is driven by turbulent diffusion which is intimately related to the vertical momentum transfer in the atmospheric boundary layer (ABL) (Wyngaard, 2010). Based on the Prandtl mixing-length theory, the shear stress can be parameterized in neutral conditions. However, it is known that for a given mean wind speed (at a reference height) in the ABL, both the mean value and the perturbations of shear stress depend on the atmospheric boundary-layer stability (ABLS), for instance, shear stress shows generally larger fluctuations in convective ABLS. Klose and Shao (2013) pointed out that:

> In a convective atmospheric boundary layer, large eddies have coherent structures of dimensions comparable to boundary-layer depth, which are efficient entities in generating localized momentum fluxes to the surface. Although the eddies only occupy fractions of time and space, the momentum fluxes to these fractions can be many times the average. (p. 49)

Hicks et al. (2016) mentioned that ABLS is of immediate concern in the micrometeorological community, because of its influences on the intermittency, gustiness and diurnal cycle of particle deposition. Similar to turbulent dust emission and intermittent sand saltation, intermittent particle deposition also occurs as a result of fluctuating surface shear stress. The current particle-deposition schemes only consider the mean behavior of wind (Slinn, 1982; Zhang and Shao, 2014; Zhang et al., 2001), and how this mean behavior varies with ABLS via the Monin-Obukhov similarity theory (Monin et al., 2007; Monin and Obukhov, 1954), but not the fluctuations of the associated shear stress and how they vary with ABLS.

We argue that focusing only on the effects of ABLS on mean wind is insufficient to accurately model particle deposition. In this study, we explore the influences of ABLS on the turbulent behavior of particle deposition and attempt to improve an existing particle deposition scheme. A large-eddy simulation (LES) model is used here to simulate turbulence and particle deposition under various ABLS conditions, and parts of the study design follow Klose and Shao (2013). The particle depositions simulated using the LES model

and predicted using the particle-deposition scheme of Zhang and Shao (2014, ZS14 hereafter) are compared with each other and with measurements. Specifically, we address the following three issues: (1) How ABLS affects the probability distribution of surface shear stress; (2) How ABLS impacts on particle deposition; and (3) How the ZS14 scheme can be improved to account for the ABLS effect. On this basis, an improvement to the ZS14 scheme (also applicable to other schemes) is proposed. The remaining part of the paper is organized as follows: Sect. 2 gives a brief description of the Weather Research and Forecast – Large-Eddy Simulation Model with Dust module (WRF-LES/D), the ZS14 scheme, and the design of the numerical experiments. Sect. 3 discusses the findings of the numerical simulations and the improvement to the ZS14 scheme. The concluding remarks are given in Sect. 4.

2. Model/Method

2.1 WRF-LES/D

The WRF-LES/D used here is initially developed by Shao et al. (2013) and Klose and Shao (2013) by coupling the WRF-LES (Moeng et al., 2007; Skamarock et al., 2008) with a land-surface module and dust module. As demonstrated in the earlier studies, WRF-LES/D is a well-established system for applications of simulating turbulence, turbulent particle emission and transport for various ABLS conditions. WRF-LES is a three-dimensional and non-hydrostatic model for fully compressible flow. The model separates the turbulent flow into a grid-resolved component and a subgrid component. The *k-l* subgrid closure (Deardorff, 1980) together with the turbulent kinetic energy (TKE) equation (Skamarock et al., 2008) is used here. The governing equations in WRF-LES/D include the equations of motion, continuity equation, enthalpy equation, equation of state and the particle conservation equation, as shown below

$$\frac{\partial u_i}{\partial t}+\frac{\partial u_i u_j}{\partial x_j}=-\delta_{i3}g+\varepsilon_{ij3}f\,u_j-\frac{1}{\rho_a}\frac{\partial p}{\partial x_i}+\nu\frac{\partial^2 u_i}{\partial x_j x_j}-\frac{1}{\rho_a}\frac{\partial \tau_{ij}}{\partial x_j} \quad (1)$$

$$\frac{\partial \rho_a}{\partial t}+\frac{\partial\left(\rho_a u_j\right)}{\partial x_j}=0 \quad (2)$$

$$\frac{\partial c_p T}{\partial t}+\frac{\partial\left(c_p u_j T\right)}{\partial x_j}=\frac{\partial H_j}{\partial x_j}+s_T \quad (3)$$

$$p=\rho_a R_a T \quad (4)$$

$$\frac{\partial c}{\partial t}+u_j\frac{\partial c}{\partial x_j}-w_t\frac{\partial c}{\partial z}=-\frac{\partial F_j}{\partial x_j}+s_r \quad (5)$$

where u_i (u, v, w) is the grid-resolved flow velocity along x_i (x, y, z) refer to the streamwise, spanwise, and vertical directions, respectively, g is the acceleration due to gravity, ρ_a is the air density, f is the Coriolis parameter, p is the air pressure, τ_{ij} is the subgrid stress tensor modeled using an eddy viscosity approach where the eddy viscosity is represented as the product of a length scale and a velocity scale characterizing

the subgrid-scale (SGS) turbulent eddies (Dupont et al., 2013), with the velocity scale being derived from the SGS TKE and the length scale from the grid spacing (Skamarock et al., 2008), v is the kinematic viscosity, δ_{i3} is the Kronecker operator and ε_{i3} is the alternating operator, c_p is the specific heat of air at constant pressure, T is air temperature, H_j is the jth component of subgrid heat flux, R_a is the specific gas constant of air, c is particle concentration, w_t is the particle terminal velocity, F_j is the jth component of subgrid particle flux, s_T and s_r are the source or sink terms for heat and particles, respectively. The subgrid eddy diffusivity is set to subgrid eddy viscosity divided by the Prandtl number. For the surface layer, an important parameterization to solve the governing equations for high-Reynolds-number turbulence is embedded in the surface boundary condition, which computes the instantaneous local surface shear stress using the bulk transfer method (Kalitzin et al., 2008; Kawai and Larsson, 2012; Piomelli et al., 2002; Zheng et al., 2020) as follows,

$$\tau = \rho_a K_m \frac{\partial V}{\partial z} \tag{6}$$

with

$$K_m = \frac{k u_* z}{\varphi_m} \tag{7}$$

where K_m is the eddy viscosity and φ_m is the MOST stability function, $V = \sqrt{u^2 + v^2}$. Even though Shao et al. (2013) questioned the application of the MOST in LES, it is still used here, as our emphasis is on the variance of shear stress in the simulation domain. Several land-surface models (LSMs) can be selected (e.g., Chen and Dudhia, 2000; Pleim and Xiu, 2003) in WRF-LES/D, and the 5-layer thermal diffusion (Dudhia, 1996) is used in this study. Furthermore, the surface heat flux, denoted H_0, is specified. The dry deposition flux to the ground for each grid, denoted F_d, is obtained by multiplying the deposition velocity V_d and particle concentration c in the lowest layer, and V_d is estimated using the ZS14 deposition scheme.

2.2 Particle-deposition scheme of ZS14

The particle deposition on the surface is more complicated than the momentum flux as the change of particle concentration close to the surface is unclear. To solve the particle conservation equation (Eq. (5)), the emission and deposition fluxes at the surface need to be specified. The problem of particle emission has been dealt with elsewhere (e.g., Shao (2004) focuses on the particle emission without turbulence effects; Klose et al., (2014) and Klose and Shao (2012) emphasize the turbulent particle emission) and is not considered here. For our purpose, particle emission is assumed to be zero. This section gives the parameterization scheme proposed by ZS14. The detail of the scheme is as described in ZS14, only the main results are given here for completeness. In general, we can express particle deposition flux F_d as

$$F_d = -\left(K_{\mathrm{p}} + k_{\mathrm{p}}\right)\frac{\partial c}{\partial z} - w_t \cdot c \tag{8}$$

where K_p and k_p are the eddy diffusivity and the molecular diffusivity, respectively. By analogy with the bulk-transfer formulation of scalar fluxes in ABL, F_d can be parameterized as

$$F_d = -V_d(z) \cdot c(z) \tag{9}$$

where $c(z)$ is the particle concentration at height z (the center height of the lowest model level in this study), $V_d(z)$ is the corresponding dry deposition velocity.

The surface layer is divided into an inertial layer and a roughness layer. Integrating Eq. (8) in the inertial layer and substituting Eq. (9) into it, $V_d(z)$ is obtained as follows:

$$V_d(z) = \left(r_g + \frac{r_s - r_g}{\exp\left(r_a / r_g\right)} \right)^{-1} \tag{10}$$

with r_g being the gravitational resistance, r_s being the collection resistance, and r_a being the aerodynamic resistance for the inertial layer.

The gravitational resistance r_g is defined as the reciprocal of the gravitational settling velocity w_t and depends mainly on particle size and density. A free-falling particle is subject to gravitational and aerodynamic drag forces. When these forces are in equilibrium, the gravitational settling velocity of the particle smaller than 20 μm can be reasonably accurately calculated according to the Stokes formula (Malcolm and Raupach, 1991; Seinfeld and Pandis, 2006).

$$w_t = \frac{C_u \rho_p D_p^2 g}{18 \mu_a} = r_g^{-1} \tag{11}$$

where D_p is the particle diameter, ρ_p is the particle density, μ_a is the air dynamic viscosity, C_u is the Cunningham correction factor that accounts for the slipping effect affecting the fine particles.

Using the MOST, the aerodynamic resistance is calculated as

$$r_a = \frac{S_{cT}}{k u_*} \left[\ln\left(\frac{z - z_d}{h - z_d} \right) - \psi_m \right] \tag{12}$$

where z_d is the displacement height, h is the height of roughness element, ψ_m is the integral of stability function in the inertial layer, $S_{cT} = K_m / K_p$ (Csanady, 1963), and κ is the von Karman constant.

In the roughness layer, the collection process is reflected in collection resistance, defined by $r_s = -\frac{c(h)}{F_d}$ with an assumption that particle concentration is zero on roughness elements or ground. In addition to the meteorological factors and land-use category, Zhang and Shao (2014) established a relationship between aerodynamic and surface-collection processes by using an analogy between drag partition and deposition flux partition, which can describe surface heterogeneity.

$$r_s^{-1} = R \cdot \frac{\tau}{\rho_a u_h}\left(\frac{E}{C_d}\frac{\tau_c}{\tau} + \left(1+\frac{\tau_c}{\tau}\right)S_c^{-1} + 10^{-\frac{3}{\hat{T}}}\right) + w_t \quad (13)$$

where R is the reduction in collection caused by particle rebound, u_h is the wind speed at the top of roughness layer, E is the collection coefficient of roughness elements and it includes the collection efficiency from Brownian motion (E_B), impaction (E_{im}) and interception (E_{in}), C_d is the drag coefficient for isolated roughness element, τ_c/τ describes the drag partition with τ_c being the pressure drag (the force exerted on roughness elements), S_c is the Schmidt number which is the ratio of air viscosity to molecular diffusion, $10^{-\frac{3}{\hat{T}}}$ represents the turbulent impaction efficiency with $\hat{T}$ being the dimensionless particle relaxation time. E_B, E_{im}, E_{in}, and R are expressed as

$$E_B = C_B S_c^{-2/3}\,\mathrm{Re}^{n_B-1} \quad (14)$$

$$E_{im} = \left(\frac{S_t}{0.6+S_t}\right)^2 \quad (15)$$

$$E_{in} = u_* 10^{-S_t}\frac{2D_p}{d_c} \quad (16)$$

$$R = \exp(-\sqrt{S_t}) \quad (17)$$

where Re is the roughness element Reynolds number, C_B and n_B are parameters depending on Re, and d_c is the diameter of the roughness element, and S_t is the Stokes number.

The ratio τ_c/τ can be calculated according to Yang and Shao (2006), as follows:

$$\frac{\tau_c}{\tau} = \frac{\beta_1\lambda_e}{1+\beta_1\lambda_e} \quad (18)$$

and

$$\lambda_e = \frac{\lambda}{(1-\eta)^6}\cdot\exp\left(-\frac{\lambda}{10\cdot(1-\eta)^6}\right) \quad (19)$$

with β_1 (= 200) being the ratio of the drag coefficient for isolated roughness element to that for bare surface, λ being the frontal area index of the roughness elements, and η being the basal area index or the fraction of cover.

From Eqs. (10) to (19), it can be seen that V_d and τ are nonlinearly related. As example, for particles with a diameter of 1 μm, analysis shows that V_d is dominated by w_t when τ is small. As τ increases, w_t and τ are both important to V_d. With τ increasing further, the effect of τ becomes much greater than gravitational settling, thus the V_d is mainly determined by τ.

2.3 Simulation Set-up

Numerical experiments are carried out with WRF-LES/D for various atmospheric stability and background-wind conditions for two different roughness lengths (Table 1). Similar to Klose and Shao (2013), the domain of the simulation is $2000 \times 2000 \times 1500$ m^3 and the number of grid points is $200 \times 200 \times 90$ corresponding to a horizontal resolution $\Delta x = \Delta y = 10$ m. The Arakawa-C staggered grid is used. The depth of the lowest model layer is 1 m and the grid above is stretched following a logarithmic function of z. The simulation time is 90 minutes with a time step of 0.05 s and the output interval is 10 s. The first 30 minutes of the simulation is the model spin-up time and the data of the remaining 60 minutes are used for the analysis.

For model initialization, the wind and particle ($\rho_p = 2650$ kg m^{-3}) concentration (Chamberlain, 1967; Monin, 1970; Kind, 1992) are assumed to be logarithmic in the vertical and uniform in the horizontal direction. For each experiment, a constant surface heat flux is specified. A 300 m deep Rayleigh damping layer is used at the upper boundary with a damping coefficient of 0.01. The wind speed at the top boundary, U, is given in Table 1. The surface heat flux, H_0, increases from -50 to 600 W m^{-2}, and for each surface heat flux, the top wind speed increase from 4 to 16 m s^{-1} in Exp (1-20) and from 5.44 to 18.12 m s^{-1} in Exp (21-35). The roughness length z_0 for sand surface used in Exp (1-20) is 0.153 mm following wind tunnel experiment (Zhang and Shao, 2014) but 0.76 mm in Exp (21-35) according to field observation (Bergametti et al., 2018). The lateral boundary conditions are periodic, which allows the simulation of a well-developed boundary layer. The vertical scaling velocity is estimated using heat flux, $w_* = \left(\frac{g}{\bar{\theta}} \frac{H_0}{\rho_a c_p} z_l \right)^{1/3}$, with $\bar{\theta}$ being the mean potential temperature and $z_l = 1000$ m is the boundary layer inversion height. Usually, w_* is not used for stable ABLS, but used here as an indicator for the suppression of turbulence by negative buoyancy.

Table 1: List of numerical experiments with $z_0 = 0.153$ mm for Exp (1-20) in wind tunnel experiments (Zhang and Shao, 2014) and $z_0 = 0.76$ mm for Exp (21-35) in field observation (Bergametti et al., 2018) for the sand surface.

$z_0 = 0.153$ mm		$z_0 = 0.76$ mm			
NAME	U (m s^{-1})	NAME	U (m s^{-1})	H_0 (W m^{-2})	w_* (m s^{-1})
EXP1	4	EXP21	5.44	-50	-1.12
EXP2	8	EXP22	10.87	-50	-1.12
EXP3	12	EXP23	18.12	-50	-1.12
EXP4	16	--	--	-50	-1.12
EXP5	4	EXP24	5.44	0	0
EXP6	8	EXP25	10.87	0	0
EXP7	12	EXP26	18.12	0	0
EXP8	16	--		0	0
EXP9	4	EXP27	5.44	200	1.77
EXP10	8	EXP28	10.87	200	1.77
EXP11	12	EXP29	18.12	200	1.77
EXP12	16	--	--	200	1.77
EXP13	4	EXP30	5.44	400	2.23

EXP14	8	EXP31	10.87	400	2.23
EXP15	12	EXP32	18.12	400	2.23
EXP16	16	--	--	400	2.23
EXP17	4	EXP33	5.44	600	2.55
EXP18	8	EXP34	10.87	600	2.55
EXP19	12	EXP35	18.12	600	2.55
EXP20	16	--	--	600	2.55

3. Results

3.1 Turbulent shear stress

In the first set of analyses, we examine the impact of atmospheric stability on shear stress fluctuations. Early particle deposition studies considered only the time average of surface shear stress, τ_r, with the assumption that shear stress is horizontally homogeneous. In WRF-LES/D, the corresponding mean resultant shear stress τ_r can be obtained as:

$$\tau_r = \sqrt{\overline{\tau}_{xz}^{\,2} + \overline{\tau}_{yz}^{\,2}} \tag{20}$$

The shorthand notation $\overline{f} = \frac{1}{N_x N_y N_t} \sum_{n_x n_y n_t} f(n_x, n_y, n_t)$ is introduced to represent the space and time average over the simulation domain and time period (hereafter ensemble mean) with N_x (=200) and N_y (=200) are the numbers of grid points in the x- and y-direction, respectively, and N_t (=360) the time steps of model output.

Figure 1a-c show the instantaneous shear stress, τ, of a sample grid (n_x = 198, n_y = 41) over a one-hour period for the runs with z_0 = 0.153 mm, U = 4 m s^{-1} and various ABL stabilities (H_0 = 0, 200, 600 W m^{-2}). Figure 1d-f is same as Fig. 1a-c, but for U = 16 m s^{-1}. The panel shows that τ is not a constant, and the mean resultant shear stress, as well as the shear stress fluctuations, increase with increasing atmospheric instability. In addition, the insert plots in Fig. 1 show that the autocorrelation function, ACF, is oscillated during decrease. The oscillation periodicity is longer under weak wind conditions (Fig. 1a-c) than strong wind (Fig. 1d-f). The ACF in neutral conditions decreases more rapidly than in convective conditions. Recall the definition of coherent motion given by Robinson (1991) - the correlation of variables over a range of long time larger than the smallest scales of flow is evidence of coherent oscillating motion. Thus, the regular oscillation and a long-time correlation of τ are closely related to the evolvement of the coherent structure. This indicates that in a convective ABL, stronger large-scale coherent structures exist even under weak wind conditions.

To gain insight into the behavior of the unsteady shear stress field, we introduce the turbulence intensity of surface shear stress (TI-S) defined as the ratio of the standard deviation of fluctuating surface shear stress, σ_τ, to the mean resultant stress τ_r, i.e., σ_τ/τ_r. Analysis shows that σ_τ/τ_r increases as atmospheric conditions become more unstable and decreases with increasing wind speed (e.g., Fig. 1). High wind speeds

tend to force the ratio to be more similar to that in neutral ABLs, as the mean-wind induced shear stress becomes dominant over the large-eddy induced shear-stress fluctuations. For a weak TI-S, τ is dominated by τ_r and the stress fluctuations are small compared to τ_r. As TI-S increases, the contribution of momentum transport by large eddies becomes significant because in unstable ABLs, buoyancy generated large eddies penetrate to high levels and intermittently enhance the momentum transfer to the surface.

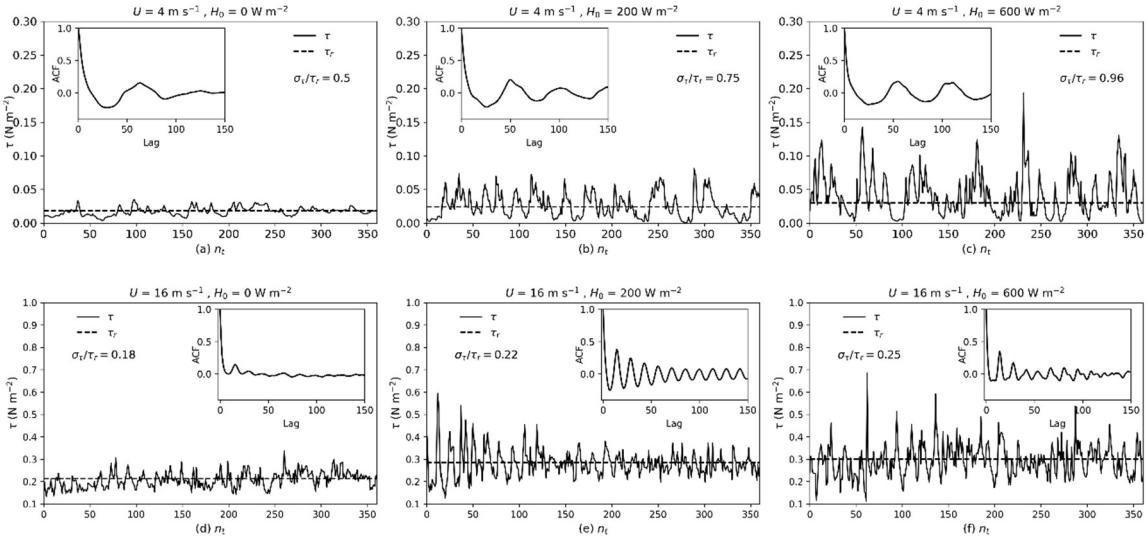

Figure 1. Time evolutions of surface shear stress τ with different H_0 values and z_0 = 0.153 mm at the grid point n_x = 198 and n_y = 41 **(a-c)** for U = 4 m s^{-1}; **(d-f)** for U = 16 m s^{-1}; the insert plots are the autocorrelation functions of τ.

The intermittent surface shear stress can directly cause localized particle deposition. Therefore, particle deposition is also intermittent in space and time. However, to our knowledge, in existing particle-deposition schemes (e.g., ZS14 used here), the particle-deposition velocity is calculated using only the mean resultant shear stress τ_r instead of the instantaneous shear stress. We denote this deposition velocity as V_{d,τ_r}. The mean deposition velocity simulated by WRF-LES/D, denoted as $V_{d,LES}$, is estimated via the ratio of the ensemble mean of particle deposition flux and the ensemble mean of particle concentration:

$$V_{d,LES} = -\frac{\overline{F}_d}{\overline{c}} \tag{21}$$

which is consistent with the methods commonly used in field observations and wind-tunnel experiments.

Figures 2a and 2b, with the same wind conditions and surface heat fluxes as in Fig.1-c and 1-f, show the time evolution of the instantaneous deposition velocity V_d for particles with a diameter of 1.46 μm. This size is chosen because it is the most sensitive to turbulent diffusion compared to the other four sizes (2.8, 4.8, 9, 16 μm) used in Exp (1-20). As shown, the fluctuating behavior of V_d is consistent with that of τ. Moreover, Fig. 2a shows a substantial difference between $V_{d,LES}$ and V_{d,τ_r}, while Fig. 2b shows V_{d,τ_r} is similar with $V_{d,LES}$. This suggests that the ZS14 scheme can more accurately estimate the deposition velocity for weak TI-S but underestimates the deposition velocity for strong TI-S. The reason for this is that

in the case of strong TI-S, particle deposition caused by the gusty wind plays an important role as V_d and τ are non-linearly related, which is not reflected in V_{d,τ_r}. Since τ fluctuates and sometimes strongly, a bias always exists in conventional particle-deposition schemes and the magnitude of the bias depends on turbulence intensity. Therefore, in order to estimate particle deposition accurately, we need to first describe and parameterize the shear stress.

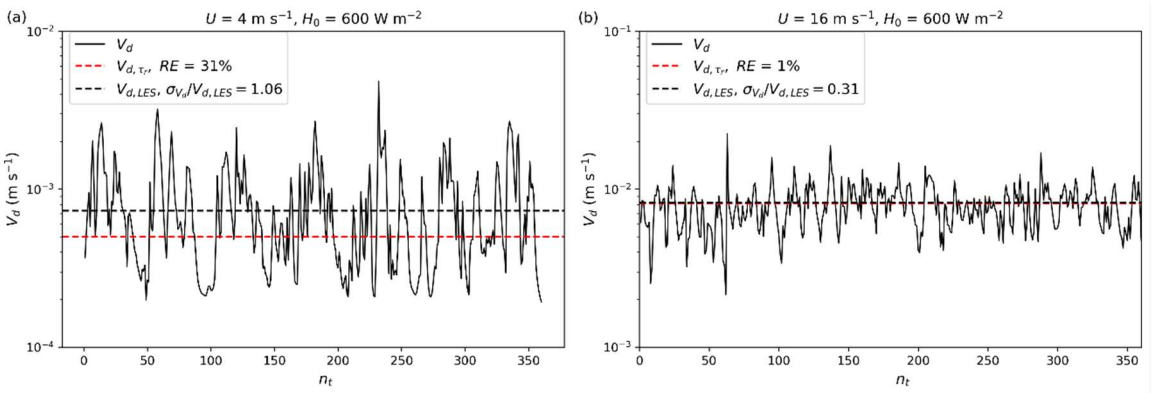

Figure 2. Time evolutions of deposition velocity V_d at grid point n_x = 198, n_y = 41 when H_0 = 600 W m^{-2}, z_0=0.153 mm and **(a)** U = 4 m s^{-1} and **(b)** U = 16 m s^{-1}. $RE = \left|\frac{V_{d,LES}-V_{d,\tau_r}}{V_{d,LES}}\right| \times 100\%$ is the relative error between V_{d,τ_r} and $V_{d,LES}$, $\sigma_{V_d}/V_{d,LES}$ is the ratio of the standard deviation of simulated instantaneous deposition velocity V_d and mean deposition velocity, $V_{d,LES}$.

As a main predisposing factor for aeolian processes, turbulent shear stress has attracted increasing attention in recent years (e.g., Klose et al., 2014; Li et al., 2020; Liu et al., 2018; Rana et al., 2020; Zheng et al., 2020). Similar to previous studies, we use the probability density function $p(\tau)$ to characterize the stochastic variable τ. Figure 3 shows that the variability of τ increases as atmospheric instability increases in different wind conditions. The statistic moments of τ, including its mean resultant value τ_r, standard deviation σ_τ, skewness γ_1 of Exp (1-20) are listed in Table 2. σ_τ and τ_r increase with increased instability, and the distribution is positively skewed. Positive skewness is characterized by the distribution having a longer positive tail as compared with the negative tail and the distribution appears as a left-leaning (i.e., tends toward low values) curve. This indicates that large negative fluctuations are not as frequent as large positive fluctuations. The data also shows γ_1 generally shows a downward trend as TI-S decreases, which is consistent with (Monahan, 2006), i.e., as TI-S decreases, $p(\tau)$ becomes increasingly Gaussian.

Table 2. Statistics of shear stress for numerical experiments Exp (1-20).

NAME	H_0	U	τ_r	σ_τ	σ_τ/τ_r	γ_1	α	β	$1/L_o$
EXP1	-50	4	0.0156	0.0086	0.554	1.902	2.026	0.011	0.475
EXP2	-50	8	0.0295	0.0096	0.327	1.573	3.154	0.023	0.153
EXP3	-50	12	0.0524	0.0115	0.22	1.029	3.923	0.044	0.06
EXP4	-50	16	0.1009	0.0158	0.157	0.835	4.819	0.09	0.02
EXP5	0	4	0.0185	0.0093	0.5	1.896	3.049	0.017	0
EXP6	0	8	0.0604	0.0151	0.25	1.142	5.004	0.055	0

EXP7	0	12	0.1315	0.0266	0.202	0.166	5.383	0.122	0
EXP8	0	16	0.2136	0.038	0.178	0.087	6.191	0.196	0
EXP9	200	4	0.024	0.018	0.75	1.142	1.56	0.025	-0.696
EXP10	200	8	0.0812	0.0325	0.4	1.02	3.022	0.076	-0.11
EXP11	200	12	0.1676	0.0451	0.269	0.512	4.078	0.156	-0.037
EXP12	200	16	0.2848	0.0624	0.219	0.766	5.214	0.259	-0.017
EXP13	400	4	0.026	0.0248	0.955	1.127	1.302	0.03	-1.258
EXP14	400	8	0.0825	0.0372	0.451	0.646	2.513	0.081	-0.216
EXP15	400	12	0.1728	0.0522	0.302	0.677	3.776	0.160	-0.071
EXP16	400	16	0.2992	0.0646	0.216	0.289	5.214	0.278	-0.031
EXP17	600	4	0.0299	0.0287	0.96	1.083	1.303	0.035	-1.575
EXP18	600	8	0.0894	0.0424	0.474	0.715	2.472	0.089	-0.29
EXP19	600	12	0.1767	0.0604	0.342	0.614	3.252	0.167	-0.103
EXP20	600	16	0.3003	0.0739	0.246	0.511	4.493	0.277	-0.046

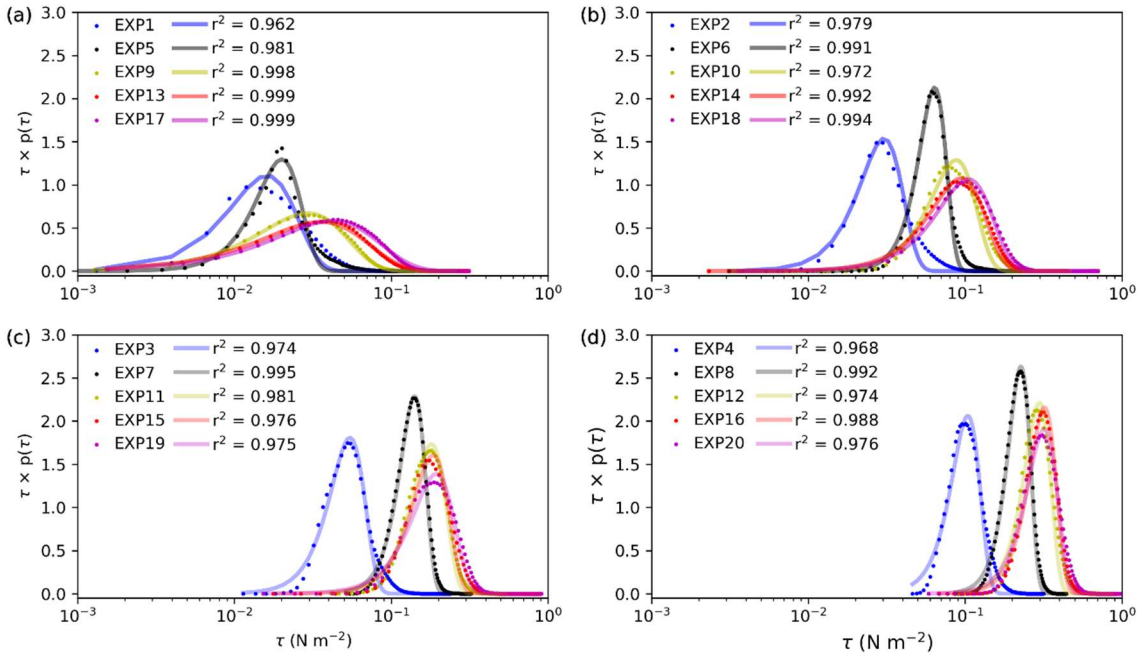

Figure 3. Probability density functions derived from WRF-LES/D simulated surface shear stress (dots) and the corresponding fitted Weibull density functions (solid lines, r^2 is the coefficients of determination) for different surface heat fluxes and different wind speeds: **(a)** U = 4 m s^{-1}, **(b)** U = 8 m s^{-1}, **(c)** U = 12 m s^{-1}, **(d)** U = 16 m s^{-1} with z_0 = 0.153 mm.

The parameterization of surface shear stress has attracted intense interests, for example, Klose et al. (2014) reported that τ in unstable conditions is Weibull distributed based on large-eddy simulations. Shao et al. (2020) found that $p(\tau)$ is skewed to small τ values (i.e., positively skewed) based on field observations. Li et al. (2020) suggested that τ in neutral conditions is Gauss distributed based on a wind-tunnel experiment. Colella and Keith (2003) explained that in turbulent shear flows, the non-linear interaction between the eddies gives rise to a departure from Gaussian behavior. Our results show that the Gaussian approximation is inadequate in representing the skewed $p(\tau)$, especially for the conditions of strong turbulence intensity (e.g., unstable cases in Fig. 3a). Therefore, $p(\tau)$ here is approximated using a Weibull distribution, i.e.,

$$p(\tau) = \frac{\alpha}{\beta}\left(\frac{\tau}{\beta}\right)^{\alpha-1} \exp\left(-(\tau/\beta)^{\alpha}\right) \tag{22}$$

where α and β are the shape and scale parameters, respectively. The α and β values of the numerical experiments Exp (1-20) are listed in Table 2. It can be seen that both α and β depend on wind speed and atmospheric stability. However, β is mainly determined by wind conditions when the wind is strong, while it is affected by ABL stability when the wind is weak. The behavior of α and β are shown in Fig. 4. $|1/L_o|$ is the absolute value of the reciprocal of the Obukhov length L_o which can be calculated by using

$$L_o = -\frac{\overline{\theta} u_*^{\,3}}{kg\dfrac{H_0}{\rho_a c_p}} \tag{23}$$

In both stable and unstable atmospheric conditions, analysis shows that the scale parameter α is related to ABL stability as the power of $|1/L_o|$. Figure 4a shows that α decreases with the $|1/L_o|$, satisfying approximately Eq. (24). For neutral conditions, L_o goes to infinity, Eq. (24) no longer applies. Therefore, the shape parameter obtained by the fitting was directly used for pdf reproduction for the neutral cases instead of the approximated α used for stable and unstable conditions. As Fig. 4b shows, the β parameter increases almost linearly with $u_{*r}^2 + 0.001 \cdot w_*^2$ but can be best approximated using Eq. (25) with $u_{*r} = \sqrt{\tau_r/\rho_a}$.

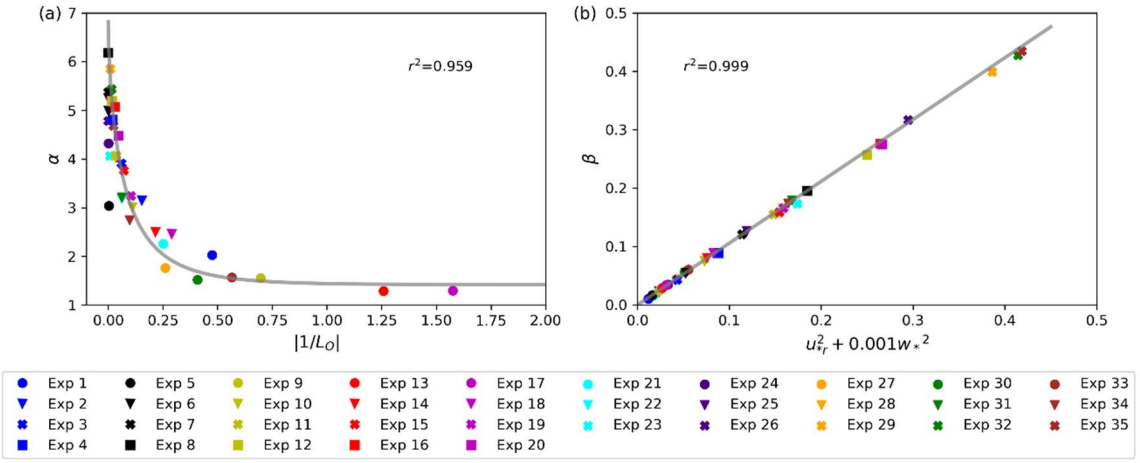

Figure 4. (a) Dependency of the shape parameter α on L_o^{-1} for all numerical experiments Exp (1-35); **(b)** Dependency of scaling parameter β on $\left(u_{*_r}{}^2 + 0.001 w_*^2\right)$ for Exp (1-35).

$$\alpha = 5.39 \cdot \exp\left(-5.43\left(\frac{1}{L_o}\right)^{2/3}\right) + 1.42 \tag{24}$$

$$\beta = 1.058 \cdot (u_{*_r}^2 + 0.001 w_*{}^2) \tag{25}$$

Using Eqs. (22)-(25), we can approximately describe the turbulent surface shear stress in non-neutral cases.

3.2 Improvement to particle deposition scheme

Figure 5a shows the performance of WRF-LES/D by comparing the simulated deposition velocity, $V_{d,LES}$, with wind tunnel experiments (Zhang and Shao, 2014) and field observation (Bergametti et al., 2018). The observed data are measured under neutral conditions and similar wind flow. As shown, the simulation results agree well with the observed data. On this basis, by further evaluating the performance of the ZS14 scheme, we found that the accuracy of the ZS14 scheme decreases with increasing instability. For example, Fig. 5b compares the deposition velocities of Exp (5, 9, 17) and Exp (24, 27, 33), $V_{d,LES}$, with those calculated by the ZS14 scheme using τ_r from the corresponding experiments, V_{d,τ_r}. It shows that under weak wind conditions, V_{d,τ_r} predicts the deposition well under neutral conditions and underestimates the deposition under convective conditions, especially for particles that are not dominated by molecular diffusion and gravity, and the underestimation increases with the atmospheric instability. To predict the deposition velocity more accurately for convective conditions, we need to account for the effect of shear-stress fluctuations, i.e., the instantaneous shear stress distribution. Thus, the dry deposition scheme can be improved as

$$V_{d,\tau} = \int_0^\infty V_d(\tau) p(\tau)\, d\tau \tag{26}$$

with $p(\tau)$ is as given by Eqs. (22)-(25). As Fig. 5c shows, the improved scheme results $V_{d,\tau}$ and the simulation value $V_{d,LES}$ are shown a remarkable congruence.

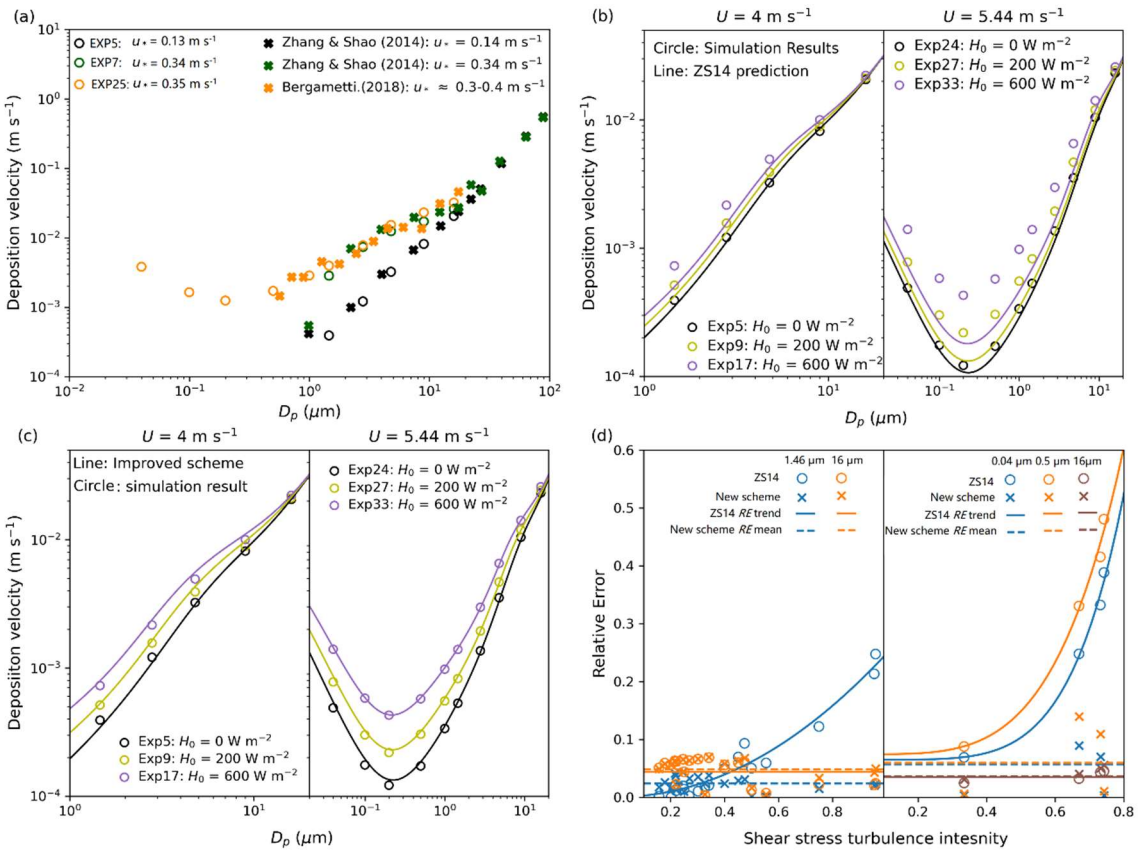

Figure 5. (a) Validation of the simulated deposition velocity from WRF-LES/D (circles) by comparing with the observation data (crosses). **(b)** the comparison of the predicted result by ZS14 scheme (lines) with the simulated value (circles) of Exp (5, 9, 17) (left) and Exp (24, 27, 33) (right). **(c)** the comparison of the predicted result by the improved scheme (lines) with the simulated value (circles) of Exp (5, 9, 17) (left) and Exp (24, 27, 33) (right). **(d)** Comparison of relative error as a function of shear stress turbulence intensity (TI-S), estimated by ZS14 scheme (circles) and the improved scheme (crosses) for Exp (1-20) (Left) and Exp (24, 27, 30, 33) (right).

To make the comparison more clear, the relative errors (*RE*) of the predicted deposition velocity by ZS14 scheme and improved scheme are compared with the WRF-LES/D simulation value and are calculated as below

$$RE = \left| \frac{V_{d,LES} - V_{d,\tau_r}\left(\text{or } V_{d,\tau}\right)}{V_{d,LES}} \right| \times 100\% \tag{27}$$

Analysis shows that the value of relative error, *RE*, depends on surface conditions, wind conditions, atmospheric stabilities, and particle sizes. It increases obviously with increased atmospheric instability under weak wind conditions, while it becomes less sensitive to stability when the wind is strong. Through the analysis, we find that the *RE* of the ZS14 scheme generally increases with the shear stress turbulence intensity, TI-S, and the value depends on particle size, as shown in Fig. 5d (left). Thus, we compared the *RE* of some different sized particles to investigate the particle in which size range is strongly affected (Fig. A2). The result shows that *RE* first increases and then decreases with increasing particle size, and the

particles with size normally in the range of 0.01 to 5 are strongly affected by turbulent shear stress and $p(\tau)$ needs to be considered. After modification, the errors are limited to less or about 10%. For example, the relative error of Exp (17, i.e., $U = 4$ m s^{-1} and $H_0 = 600$ W m^{-2}) for particles of 1.46 μm is reduced from ~ 25% to ~ 3%. The relative error of Exp (33, i.e., $U = 5.44$ m s^{-1}and $H_0 = 600$ W m^{-2}) for particles of 0.5 μm is reduced from ~ 50% to ~ 12%.

To further analyze if the *RE* of ZS14 in unstable conditions is dominated by kinetic instability or dynamic instability, the Richardson number is calculated. Analysis shows that TI-S is positively correlated to gradient Richardson number Ri (Eq. A1). Under unstable conditions associated with strong vertical motion and weak winds, the *RE* of ZS14 increases with the increasing magnitude of Richardson number Ri (Fig. A3). The relationship between Ri and TI-S needs further study. Consequently, the results illustrate that the modified scheme $V_{d,\tau}$ tends to be more accurate than the unmodified scheme V_{d,τ_r}.

4. Conclusion

The present study was designed to determine the effect of ABL stability on particle deposition. For this purpose, the WRF-LES/D was used to model atmospheric boundary-layer turbulence under the presence of atmospheric stability effects to recover statistics of shear stress variability. We then presented an improved particle-deposition scheme with the consideration of turbulent shear stress. While ABLS can broadly represent levels of atmospheric turbulence, its effect on particle deposition is wind speed dependent. Through a series of numerical experiments, we have shown the turbulent characteristics of particle deposition velocity caused by the turbulent wind flow and pointed out the shortcomings of the ZS14 scheme in representing particle deposition under convective conditions. The relative error *RE* increases as the ABL instability increases for low wind conditions, i.e., *RE* increases with shear stress turbulence intensity, especially for a certain size range of particles.

Since the dependency of particle deposition on micrometeorology is embedded in the application of the surface shear stress, we believe that the dependency of particle deposition on ABL stability is ultimately attributed to the statistical behavior of shear stress τ. Therefore, in this study, a model including the effects of surface shear fluctuations is proposed and validated by numerical experiments. Additionally, the fluctuations of surface shear caused by turbulence can be approximated with a Weibull distribution. The shape parameter decreases exponentially with the reciprocal of Monin-Obukhov length, and the scale parameter increases linearly with $u_{*r}^2 + 0.001w_*^2$. After statistically revising the original scheme, an improved model is obtained. Using the modified model, the deposition velocity tends towards numerical experimental results.

The project is the first comprehensive investigation of the turbulent characters of particle deposition and the findings will be of interest to improve the accuracy of particle-deposition predictions on regional or global scales. One source of weakness in this study is the variation of τ may be changed by surface roughness and

needs further study, as the roughness length does not fully reflect the effect of the surface topography on the turbulence structure. In spite of this limitation, the study adds to our understanding of the influence caused by ABLS on particle deposition.

Appendix

Figure A1 shows the probability density distribution of surface shear stress for experiments (21-35); Figure A2 shows the changing of relative error with particle size; Figure A3 shows the variation of relative error (*RE*) of the ZS14 scheme (Eq. (10)) and improved scheme (Eq. (26)) with gradient Richardson number Ri.

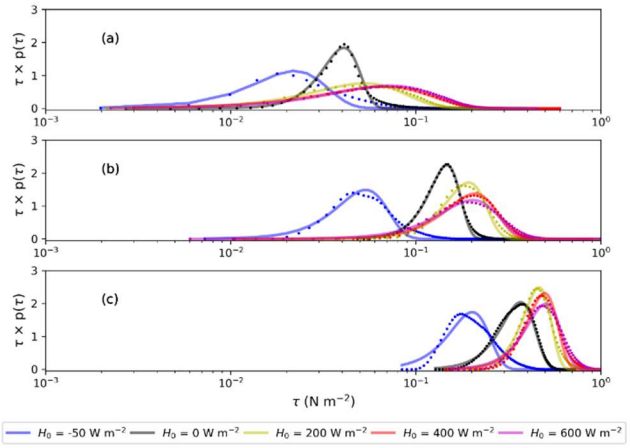

Figure A1. Probability distributions of simulated surface shear stress (dots) and the corresponding fitted Weibull density distribution (solid lines) with different surface heat flux for different wind conditions: **(a)** U = 5.44 m s^{-1}, **(b)** U = 10.87 m s^{-1}, **(c)** U = 18.12 m s^{-1}.

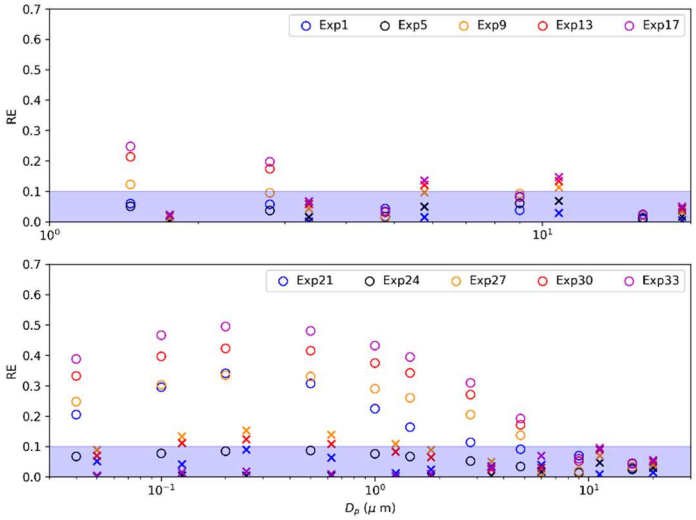

Figure A2. *RE* changes with particle size under weak wind conditions.

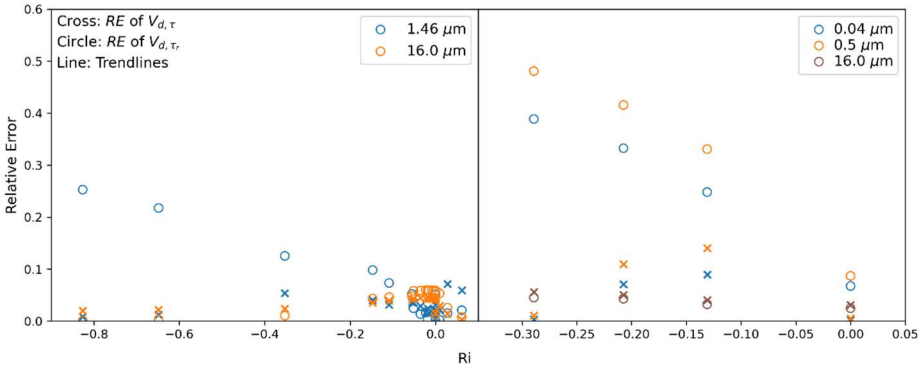

Figure A3. Comparison of relative error as a function of Ri, estimated by ZS14 scheme (circles) and the improved scheme (crosses) for Exp (1-20) (left) and Exp (24, 27, 30, 33) (right).

$$R_i = -\frac{g}{\bar{\theta}} kz \frac{\varphi_h}{\varphi_m^2} \frac{H_0}{\rho_a c_p u_*^3} \tag{A1}$$

where z is the center height of the lowest layer, $\bar{\theta}$ is the potential temperature of the lowest layer.

Code and data availability

The source code used in this study is the WRF-chem version 3.7 in the LES mode coupled with a new deposition scheme. WRF-LES model can be downloaded at https://www2.mmm.ucar.edu/wrf/users/download/get_sources.html. The code of the coupled deposition scheme and data set obtained by the simulation are available online at https://github.com/YinXin2021/WRF-LES-DustDepositionScheme.

Author contributions

XY, YP and JZ were responsible for the formal analysis, Methodology. XY and CJ were responsible for the data curation, software, validation and visualization. YP, JZ and NH were responsible for the supervision, project administration and funding acquisition. XY was responsible for investigation and Writing - original draft preparation. XY, YP, JZ and CJ were responsible for the Writing – review & editing.

Competing interests

The authors declare that they have no conflict of interest.

Disclaimer

Publisher's note: Copernicus Publications remains neutral with regard to jurisdictional claims in published maps and institutional affiliations.

Acknowledgments

We thank the Second Tibetan Plateau Scientific Expedition and Research Program (2019QZKK020611)，the State Key Program of the National Natural Science Foundation of China (41931179), the China Scholarship Council (No. 201606180041) and the Fundamental Research Funds for the Central Universities (grant no. lzujbky-2020-cd06), the Major Science and Technology Project of Gansu Province (21ZD4FA010).

References

Bergametti, G., Marticorena, B., Rajot, J. L., Foret, G., Alfaro, S. C. and Laurent, B.: Size-Resolved Dry Deposition Velocities of Dust Particles: In Situ Measurements and Parameterizations Testing, J. Geophys. Res. Atmos., 123(19), 11,080-11,099, doi:10.1029/2018JD028964, 2018.

Chamberlain, A. C.: Aspects of travel and deposition of aerosol and vapour clouds, U.K., 1953.

Chamberlain, A. C.: Transport of Lycopodium spores and other small particles to rough surfaces, Proc. R. Soc. London. Ser. A. Math. Phys. Sci., 296, 45–70, doi:10.1098/rspa.1967.0005, 1967.

Chen, S. H. and Dudhia, J.: Annual report: WRF physics, Air Force Weather Agency, (January 2000), 1–38, 2000.

Colella, K. J. and Keith, W. L.: Measurements and scaling of wall shear stress fluctuations, Exp. Fluids, 34(2), 253–260, doi:10.1007/s00348-002-0552-2, 2003.

Connan, O., Pellerin, G., Maro, D., Damay, P., Hébert, D., Roupsard, P., Rozet, M. and Laguionie, P.: Dry deposition velocities of particles on grass: Field experimental data and comparison with models, J. Aerosol Sci., 126(November 2017), 58–67, doi:10.1016/j.jaerosci.2018.08.004, 2018.

Csanady, G. T.: Turbulent Diffusion of Heavy Particles in the Atmosphere, J. Atmos. Sci., 20, 201–208, doi:10.1175/1520-0469(1964)021<0322:codohp>2.0.co;2, 1963.

Damay, P. E., Maro, D., Coppalle, A., Lamaud, E., Connan, O., Hébert, D., Talbaut, M. and Irvine, M.: Size-resolved eddy covariance measurements of fine particle vertical fluxes, J. Aerosol Sci., 40(12), 1050–1058, doi:10.1016/j.jaerosci.2009.09.010, 2009.

Deardorff, J. W.: Stratocumulus-capped mixed layers derived from a three-dimensional model, Boundary-Layer Meteorol., 18(4), 495–527, doi:10.1007/BF00119502, 1980.

Droppo, J. G.: Improved Formulations for Air-Surface Exchanges Related to National Security Needs: Dry Deposition Models., Richland, WA., 2006.

Dudhia, J.: A multi-layer soil temperature model for MM5, Prepr. from Sixth PSU/NCAR Mesoscale Model Users' Work. 22-24 July 1996, Boulder, Color., 1996.

Dupont, S., Bergametti, G., Marticorena, B. and Simoëns, S.: Modeling saltation intermittency, J. Geophys. Res. Atmos., 118(13), 7109–7128, doi:10.1002/jgrd.50528, 2013.

Fowler, D., Pilegaard, K., Sutton, M. A., Ambus, P., Raivonen, M., Duyzer, J., Simpson, D., Fagerli, H., Fuzzi, S., Schjoerring, J. K., Granier, C., Neftel, A., Isaksen, I. S. A., Laj, P., Maione, M., Monks, P. S., Burkhardt, J., Daemmgen, U., Neirynck, J., Personne, E., Wichink-Kruit, R., Butterbach-Bahl, K., Flechard, C., Tuovinen, J. P., Coyle, M., Gerosa, G., Loubet, B., Altimir, N., Gruenhage, L., Ammann, C., Cieslik, S., Paoletti, E., Mikkelsen, T. N., Ro-Poulsen, H., Cellier, P., Cape, J. N., Horváth, L., Loreto, F., Niinemets, Ü., Palmer, P. I., Rinne, J., Misztal, P., Nemitz, E., Nilsson, D., Pryor, S., Gallagher, M. W., Vesala, T., Skiba, U., Brüggemann, N., Zechmeister-Boltenstern, S., Williams, J., O'Dowd, C., Facchini, M. C., de Leeuw, G., Flossman, A., Chaumerliac, N. and Erisman, J. W.: Atmospheric composition change: Ecosystems-Atmosphere interactions, Atmos. Environ., 43(33), 5193–5267, doi:10.1016/j.atmosenv.2009.07.068, 2009.

Gregory, P. H.: The dispersion of air-borne spores, Trans. British Mycological Soc., 28(1-2), 26-72, doi:10.1016/s0007-1536(45)80041-4, 1945.

Hicks, B. B., Saylor, R. D. and Baker, B. D.: Dry deposition of particles to canopies-A look back and the road forward, J. Geophys. Res., 121(24), 14691–14707, doi:10.1002/2015JD024742, 2016.

Kalitzin, G., Medic, G. and Templeton, J. A.: Wall modeling for LES of high Reynolds number channel flows: What turbulence information is retained?, Comput. Fluids, 37(7), 809–815, doi:10.1016/j.compfluid.2007.02.016, 2008.

Kawai, S. and Larsson, J.: Wall-modeling in large eddy simulation: Length scales, grid resolution, and accuracy, Phys. Fluids, 24(1), doi:10.1063/1.3678331, 2012.

Kind, R. J.: One-dimensional aeolian suspension above beds of loose particles-A new concentration-profile equation, Atmos. Environ. Part A, Gen. Top., 26(5), 927–931, doi:10.1016/0960-1686(92)90250-O, 1992.

Klose, M. and Shao, Y.: Stochastic parameterization of dust emission and application to convective atmospheric conditions, Atmos. Chem. Phys., 12(16), 7309–7320, doi:10.5194/acp-12-7309-2012, 2012.

Klose, M. and Shao, Y.: Large-eddy simulation of turbulent dust emission, Aeolian Res., 8, 49–58, doi:10.1016/j.aeolia.2012.10.010, 2013.

Klose, M., Shao, Y., Li, X., Zhang, H., Ishizuka, M., Mikami, M. and Leys, J. F.: Further development of a parameterization for convective turbulent dust emission and evaluation based on field observations, J. Geophys. Res., 119(17), 10441–10457, doi:10.1002/2014JD021688, 2014.

Lamaud, E., Chapuis, A., Fontan, J. and Serie, E.: Measurements and parameterization of aerosol dry deposition in a semi-arid area, Atmos. Environ., 28(15), 2461–2471, doi:10.1016/1352-2310(94)90397-2, 1994.

Li, G., Zhang, J., Herrmann, H. J., Shao, Y. and Huang, N.: Study of Aerodynamic Grain Entrainment in Aeolian Transport, Geophys. Res. Lett., 47(11), doi:10.1029/2019GL086574, 2020.

Liu, D., Ishizuka, M., Mikami, M. and Shao, Y.: Turbulent characteristics of saltation and uncertainty of saltation model parameters, Atmos. Chem. Phys., 18(10), 7595–7606, doi:10.5194/acp-18-7595-2018, 2018.

Malcolm, L. P. and Raupach, M. R.: Measurements in an air settling tube of the terminal velocity distribution of soil material, J. Geophys. Res., 96, 15,275-15,286, 1991.

Moeng, C.-H., Dudhia, J., Klemp, J. and Sullivan, P.: Examining Two-Way Grid Nesting for Large Eddy Simulation of the PBL Using the WRF Model, Mon. Weather Rev., 135(6), 2295–2311, doi:10.1175/MWR3406.1, 2007.

Monahan, A. H.: The probability distribution of sea surface wind speeds. Part I: Theory and SeaWinds observations, J. Clim., 19(4), 497–520, doi:10.1175/JCLI3640.1, 2006.

Monin, A. S.: The Atmospheric Boundary Layer, Annu. Rev. Fluid Mech., 2(1), 225–250, doi:10.1146/annurev.fl.02.010170.001301, 1970.

Monin, A. S. and Obukhov, A. M.: Basic Laws of Turbulence Mixing in the Ground Layer of the Atmosphere, Tr. Akad. Nauk. SSSR Geophiz. Inst., 24(151), 1954.

Monin, A. S., I?A?glom, A. M. and Lumley, J. L.: Statistical Fluid Mechanics: Mechanics of Turbulence, Dover Publications. [online] Available from: https://books.google.de/books?id=EtTyyI4%5C_DvIC, 2007.

Pellerin, G., Maro, D., Damay, P., Gehin, E., Connan, O., Laguionie, P., Hébert, D., Solier, L., Boulaud, D., Lamaud, E. and Charrier, X.: Aerosol particle dry deposition velocity above natural surfaces: Quantification according to the particles diameter, J. Aerosol Sci., 114, 107–117, doi:10.1016/j.jaerosci.2017.09.004, 2017.

Petroff, A. and Zhang, L.: Development and validation of a size-resolved particle dry deposition scheme for application in aerosol transport models, Geosci. Model Dev., doi:10.5194/gmd-3-753-2010, 2010.

Piomelli, U., Balaras, E., Squires, K. D. and Spalart, P. R.: Zonal approaches to wall-layer models for large-eddy simulations, in 3rd Theoretical Fluid Mechanics Meeting., 2002.

Pleim, J. E. and Xiu, A.: Development of a land surface model. Part II: Data assimilation, J. Appl. Meteorol., 42(12), 1811–1822, doi:10.1175/1520-0450(2003)042<1811:DOALSM>2.0.CO;2, 2003.

Rana, S., Anderson, W. and Day, M.: Turbulence-Based Model for Subthreshold Aeolian Saltation, Geophys. Res. Lett., 47(15), 1–9, doi:10.1029/2020GL088050, 2020.

Robinson, S. K.: Coherent motions in the turbulent boundary layer, Annu. Rev. Fluid Mech., 23(1), doi:10.1146/annurev.fl.23.010191.003125, 1991.

Sehmel, G. A.: Particle and gas dry deposition: A review, Atmos. Environ., 14(9), 983–1011, doi:10.1016/0004-6981(80)90031-1, 1980.

Seinfeld, J. H. and Pandis, S. N.: Atmospheric Chemistry and Physics: From Air Pollution to Climate Change, Wiley. [online] Available from: https://books.google.de/books?id=tZEpAQAAMAAJ, 2006.

Seinfeld, J. H., Bretherton, C., Carslaw, K. S., Coe, H., DeMott, P. J., Dunlea, E. J., Feingold, G., Ghan, S., Guenther, A. B., Kahn, R., Kraucunas, I., Kreidenweis, S. M., Molina, M. J., Nenes, A., Penner, J. E., Prather, K. A., Ramanathan, V., Ramaswamy, V., Rasch, P. J., Ravishankara, A. R., Rosenfeld, D.,

Stephens, G. and Wood, R.: Improving our fundamental understanding of the role of aerosol−cloud interactions in the climate system, Proc. Natl. Acad. Sci., 113(21), 5781–5790, doi:10.1073/PNAS.1514043113, 2016.

Shao, Y.: Simplification of a dust emission scheme and comparison with data, J. Geophys. Res. D Atmos., 109(10), 1–6, doi:10.1029/2003JD004372, 2004.

Shao, Y., Liu, S., Schween, J. H. and Crewell, S.: Large-Eddy Atmosphere-Land-Surface Modelling over Heterogeneous Surfaces: Model Development and Comparison with Measurements, Boundary-Layer Meteorol., 148(2), 333–356, doi:10.1007/s10546-013-9823-0, 2013.

Shao, Y., Zhang, J., Ishizuka, M., Mikami, M., Leys, J. and Huang, N.: Dependency of particle size distribution at dust emission on friction velocity and atmospheric boundary-layer stability, Atmos. Chem. Phys., 20(21), 12939–12953, doi:10.5194/acp-20-12939-2020, 2020.

Skamarock, W. C., Klemp, J. B., Dudhi, J., Gill, D. O., Barker, D. M., Duda, M. G., Huang, X.-Y., Wang, W. and Powers, J. G.: A Description of the Advanced Research WRF Version 3, Tech. Rep., (June), 113, doi:10.5065/D6DZ069T, 2008.

Slinn, S. A. and Slinn, W. G. N.: Predictions for particle deposition on natural waters, Atmos. Environ., 14(9), 1013–1016, doi:10.1016/0004-6981(80)90032-3, 1980.

Slinn, W. G. N.: Predictions for particle deposition to vegetative canopies, Atmos. Environ., 16(7), 1785–1794, doi:10.1016/0004-6981(82)90271-2, 1982.

Walcek, C. J., Brost, R. A., Chang, J. S. and Wesely, M. L.: SO2, sulfate and HNO3 deposition velocities computed using regional landuse and meteorological data, Atmos. Environ., 20(5), 949–964, doi:10.1016/0004-6981(86)90279-9, 1986.

Wesely, M. L., Cook, D. R. and Hart, R. L.: Fluxes of gases and particles above a deciduous forest in wintertime, Boundary-Layer Meteorol., 27(3), 237–255, doi:10.1007/BF00125000, 1983.

Wesely, M. L., Cook, D. R. and Hart, R. L.: Measurements and parameterization of particulate sulfur dry deposition over grass., J. Geophys. Res., doi:10.1029/jd090id01p02131, 1985.

Wyngaard, J. C.: Turbulence in the atmosphere., 2010.

Yang, Y. and Shao, Y.: A scheme for scalar exchange in the urban boundary layer, Boundary-Layer Meteorol., 120(1), 111–132, doi:10.1007/s10546-005-9033-5, 2006.

Zhang, J. and Shao, Y.: A new parameterization of particle dry deposition over rough surfaces, Atmos. Chem. Phys., 14(22), 12429–12440, doi:10.5194/acp-14-12429-2014, 2014.

Zhang, J., Shao, Y. and Huang, N.: Wind-tunnel experiment on dust dry deposition, in AIP Conference Proceedings., 2013.

Zhang, L., Gong, S., Padro, J. and Barrie, L.: A size-segregated particle dry deposition scheme for an atmospheric aerosol module, Atmos. Environ., doi:10.1016/S1352-2310(00)00326-5, 2001.

Zheng, X., Jin, T. and Wang, P.: The Influence of Surface Stress Fluctuation on Saltation Sand Transport Around Threshold, J. Geophys. Res. Earth Surf., 125(5), 0–2, doi:10.1029/2019JF005246, 2020.

555